Numerical implementation of multiple peeling theory and its application to spider web anchorages

Numerical validation of Multiple Peeling Theory and its application to spider-web anchorages

Lucas Brely[(1)], Federico Bosia[(1)], and Nicola M. Pugno[(2,3,4)*]

(1) Department of Physics and "Nanostructured Interfaces and Surfaces" Centre, Università di Torino, Via P. Giuria 1, 10125, Torino (Italy).

(2) Laboratory of Bio-Inspired & Graphene Nanomechanics, Department of Civil, Environmental and Mechanical Engineering, Università di Trento, via Mesiano, 77, I-38123 Trento, Italy.

(3) Center for Materials and Microsystems, Fondazione Bruno Kessler, Via Sommarive 18, I-38123 Povo (Trento), Italy.

(4) School of Engineering and Materials Science, Queen Mary University of London, Mile End Road, London E1 4NS.

(*) Corresponding author: *nicola.pugno@unitn.it*

Abstract: Adhesion of spider web anchorages has been studied in recent years, including the specific functionalities achieved through different architectures. To better understand the delamination mechanisms of these and other biological or artificial fibrillar adhesives, and how their adhesion can be optimized, we develop a novel numerical model to simulate the multiple peeling of structures with arbitrary branching and adhesion angles, including complex architectures. We validate the numerical model by comparing predictions with the recently developed Multiple Peeling Theory (MPT), which extends the energy-based single peeling theory of Kendall, finding excellent agreement even for complex structures. In particular we numerically confirm that a multiple peeling problem can be treated as the superposition of single peeling configurations even for complex structures. Finally, we apply the developed numerical approach to study spider web anchorages, showing how their function is achieved through optimal geometrical configurations.

Keywords: Adhesion, Numerical simulations, Multiple peeling, Spider web anchorages.

PACS numbers:

Mechanical properties of nanoscale systems, 62.25.-g

Nanoscale materials, structure of, 61.46.-w,

Computer modeling and simulation, 07.05.Tp

Nanoscale systems, fracture, 62.25.Mn

1. Introduction

Natural adhesives have captured considerable interest in recent years due to their outstanding mechanical properties [1]. Well-known examples are gecko or insect adhesion [2, 3], or spider-web attachments [4], in which geometry, structure and material properties are essential in defining functionality. Gecko adhesion, which is based on Van Der Waals forces, achieves strengths of up to 1 MPa through the contact of billions of spatulae for each foot pad [5, 6]. As in other cases of natural adhesives, the key to strong adhesion seems to lie in their hierarchical structure, which allows good adaptation to the surface and repeated contact splitting to increase the total peeling line without self-bunching [7, 8]. The observation of these natural structures has inspired the design and realization of artificial dry adhesives (i.e. based on Van der Waals forces) that guarantee simultaneous strong adhesion and smart, easy release, usually realized in polymers by means of "mushroom-shaped" terminal elements tens of micrometers in size [9-13]. These structures, like gecko or insect terminal elements (spatulae), are tapered in shape [7], so that their detachment from the surface is reminiscent of the peeling of a tape from a substrate. Multiple Peeling Theory (MPT) has recently been introduced by Pugno, and applied to cases of interest such as the delamination of a V-shaped elastic tape from a substrate, or to spider web anchorages [14, 15].

The theory is a generalization of the well-known single peeling theory by Kendall [16], and predicts a critical value of the pull-off force corresponding to a limiting peeling angle which is reached as the delamination advances. Both the pull-off force and limiting angle only depend on the geometry of the tape, its elastic modulus and the

interfacial energy. In [14], Pugno formulates an assumption (“ansatz”) relating multiple to single peeling theory, as he theoretically demonstrated for the symmetric double peeling, stating that any multiple peeling problem can be treated as the superposition of single peeling ones, using Kendall’s theory or its extensions. In this paper, we numerically demonstrate the validity of this hypothesis.

MPT is particularly useful to study the geometries of cases of interest found in Nature, where evolution has encouraged optimization of structure and material properties for specific functions [17]. Spider web anchorages are one relevant case. For example, Sahni et al. recently discussed the case of different attachment disks for cobweb-weaving spiders, showing that the attachment strengths of the different configurations (“scaffolding” and “gumfoot” silk), are related to their specific function, namely locomotion and prey capture [18]. Also, Pugno et al. compared multiple peeling theory with atomistic modeling to demonstrate a synergy between material constitutive law and structural geometry, similarly to their previous findings on spider webs [19]. In this paper we introduce a novel energy-based numerical model to address complex multiple peeling problems, including asymmetrical geometries or loading configurations. Results validate and complement those obtained in previous studies and further clarify optimization mechanisms, analysing specific attachment disk configurations and adding further elements to interpret their particular structure.

The paper is structured as follows: in Section 2, the numerical model is outlined; in Section 3.1, the model is validated by comparing its predictions to known MPT results and further simulations regarding a symmetric double peeling configuration are presented; in Sections 3.2 and 3.3, results relative to asymmetrical double peeling geometries are discussed, leading to a generalization of the multiple peeling problem;

finally, in Section 4, the results from previous sections are used to analyse two of the most common spider web anchorages and interpret their structure on the basis of their function.

2. Numerical model

We wish to consider a model anchorage constituted by multiple tapes converging to a single point (or line), undergoing detachment by simultaneous or sequential peeling of the various tapes, and evaluate the adhesive properties of the system as a function of the specific configuration. To do this, we adopt a 2-D semi-analytical model based on discrete nodal displacements: each tape is considered as a truss element of variable length, depending on the delaminated length, and each node has 2 degrees of freedom. As a first approximation, material the constitutive law is considered to be isotropic and linear elastic.

The simplest case is a V-shaped double peeling configuration, shown in Fig.1, in which 3 nodes are necessary. An imposed displacement is incrementally applied on the structure vertex. For each increment, the balance between elastic energy and adhesive energy is computed between the deformed state and the delaminated state, assuming a discrete delamination length l_{del}. The external work term is absent since the simulation is in displacement control, so that when delamination occurs, the position of the application of the force remains constant. Using the indices I, II and III for initial, deformed and delaminated states, respectively, delamination of the tapes i=1, 2 takes place when the stored elastic energy exceeds the energy needed to create a new area of surface $b \cdot l_{del}$ [14]:

$$\frac{1}{2} YA \left[\frac{(l_{II,i} - l_{I,i})^2}{l_{I,i}} - \frac{(l_{III,i} - l_{I,i} - l_{del})^2}{l_{I,i} + l_{del}} \right] = bRl_{del} \qquad (1)$$

where Y is the tape Young's modulus, A its cross section, b its width, l its length and R the adhesive energy per unit area. Tape tensions (f_i) and therefore the total external load F corresponding to the imposed displacement can be calculated from tape deformations Δl_i using Hooke's law:

$$f_i = YA\frac{\Delta l_i}{l_i} \tag{2}$$

The iterative process continues after delamination, considering the modified system configuration, i.e. attachment node displacements and tape length increments (as shown in Fig. 1).

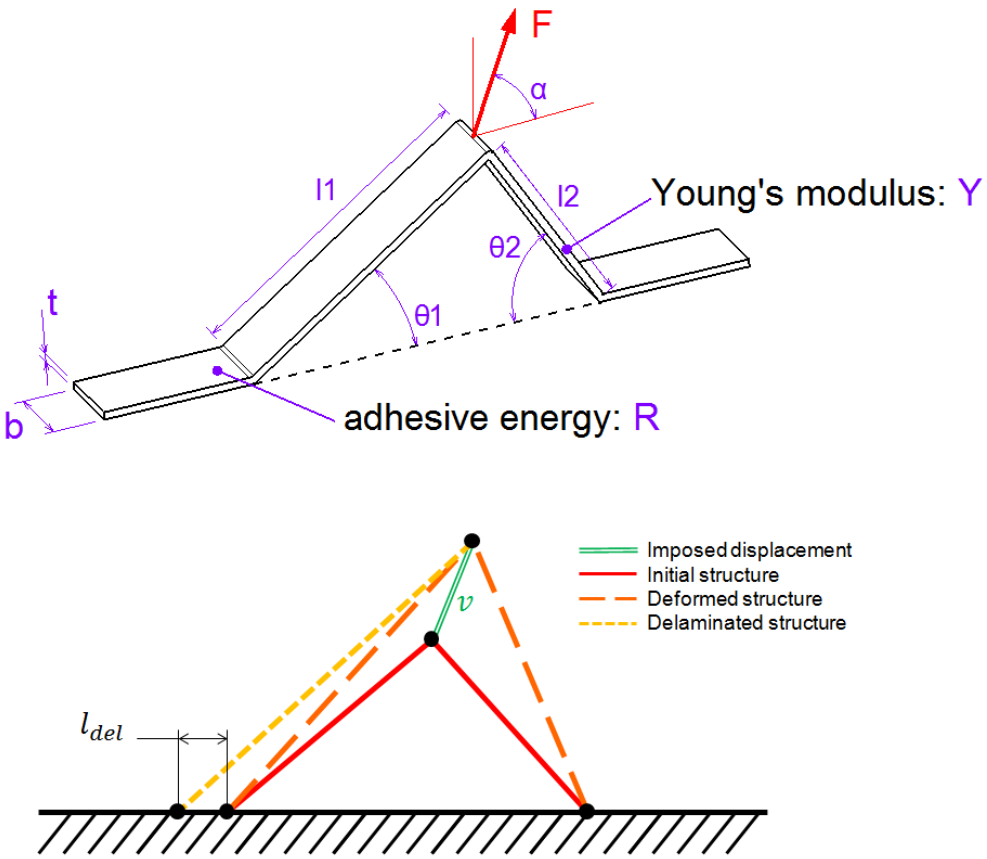

Fig. 1: (Above) Schematic geometry of an asymmetrical double-peeling configuration. (Below) Comparison between initial, deformed and delaminated configurations. For simplicity, delamination is shown on only one of the two branches.

3. Model results: double peeling

3.1 Symmetrical loading of a double peeling symmetric configuration

We first discuss a symmetrical peeling geometry with purely vertical loading (referring to Fig. 1: $l_1 = l_2 = l$, $\theta_1 = \theta_2 = \theta$, $\alpha = 90°$). The chosen geometrical and mechanical properties of the tape are $t = 0.125$ mm, $b = 15$ mm, $Y = 3$ MPa, $\nu = 0.5$, $l = 100$ mm. To begin with, we study the deformation of the structure only up to the onset of delamination. For different values of

adhesive strength R, Fig. 2 shows the numerical predictions of the normalized force $F(\theta)/F(\pi/2)$ necessary to obtain delamination of the tapes as a function of the peeling angle θ (i.e the angle of the deformed tape with respect to the surface at which delamination occurs). These numerical results can be compared to analytical predictions using MPT [14], which in turn extends Kendall's single peeling theory [16]. Accordingly, the energy balance (as described in Section 2) for the peeling of a single tape is:

$$\frac{f^2}{2btY} + f(1 - \cos(\theta)) - bR = 0 \tag{3}$$

The analytical expression for the single peeling force is therefore:

$$f = btY\left[\cos(\theta) - 1 + \sqrt{(1 - \cos(\theta))^2 + \frac{2R}{tY}}\right] \tag{4}$$

In this symmetrical case, Pugno [14] showed that the total delamination force can also be obtained as the sum of two single peeling forces using Kendall's equations [16]

$$F = 2\sin(\theta)\, f \tag{5}$$

Analytical values using eqs. (4) and (5) are also plotted in Fig. 2 together with numerical predictions for different values, showing a perfect overlap. These results show that an optimal peeling angle is reached before delamination, in correspondence with which the peeling force is maximum, which depends on the adhesive energy of the tape-substrate. Numerical solutions do not appear on the descending branch of the analytic curves, for peeling angles smaller than

this optimal angle. This is because, as we show below, optimal peeling angles (curve maxima) correspond to zero non-deformed (initial) angles, and thus smaller peeling angles would correspond to negative initial angles, which is physically meaningless [15].

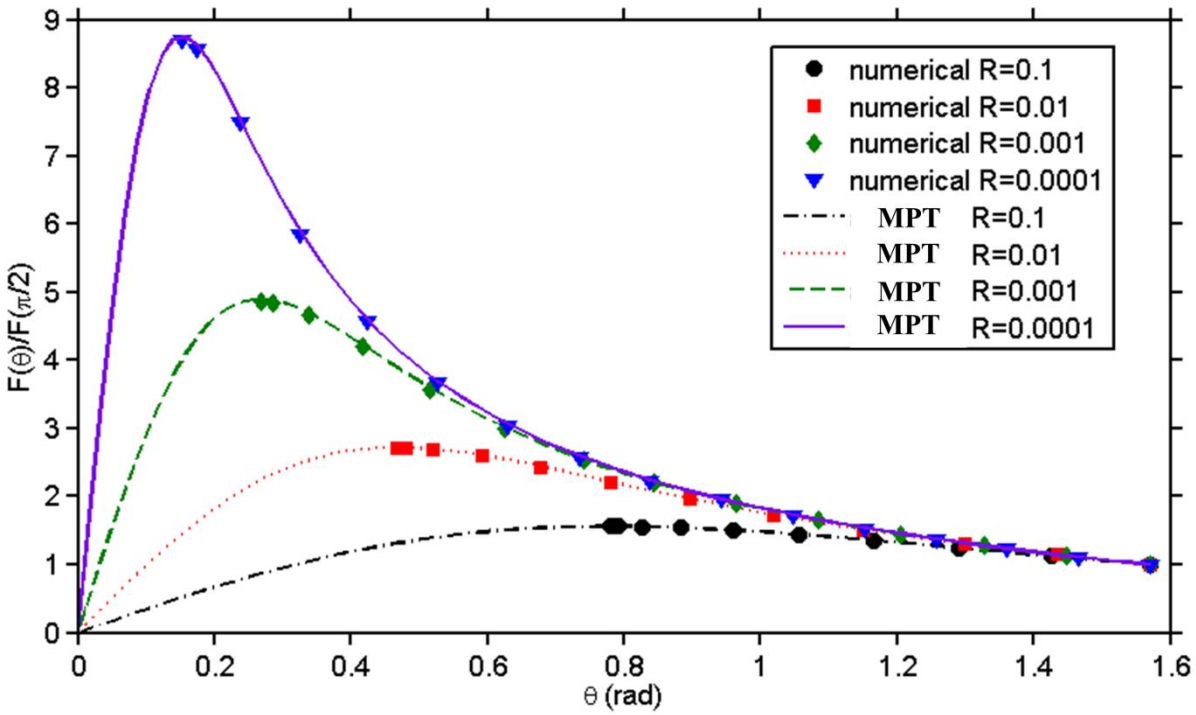

Fig. 2: Analytically (MPT) and numerically calculated results for normalized delamination load $F(\theta)/F(\pi/2)$ vs. peeling angle θ in a symmetrical double peeling configuration for various adhesive energies R (in J/mm²)

Referring to Fig. 1, if deformation starts from an initial angle θ_0, after deformation the strain in each of the two tapes is $\varepsilon = \Delta L/L = \cos\theta_0/\cos(\theta) - 1$. Therefore, the tape tension can be expressed as:

$$f = btY\left(\frac{\cos\theta_0}{\cos\theta} - 1\right) \tag{6}$$

while the vertical external load at the vertex of the two tapes is expressed by eq. (5). It is clear then that the optimal peeling force is obtained for $\theta_0 = 0$, as shown in Fig. 3a: the corresponding curve intersects the peeling force curve at its maximum value (the same mechanical properties as previously are used). We thus plot in Fig. 3b the external load F for $\theta_0 = 0$ as a function of the peeling angle θ as derived from eqs. (5) and (6), together with the peeling forces previously shown in Fig. 2 for various R values. The intersections between the curves, which correspond to the F values for which tapes with different R values delaminate, occur in all cases at the maximum of the peeling force curves, i.e. for optimal peeling angle values. This result confirms the fact that peeling cannot occur for the angle values below the optimal angle, since the tape tension for these angles is smaller than that necessary to delaminate.

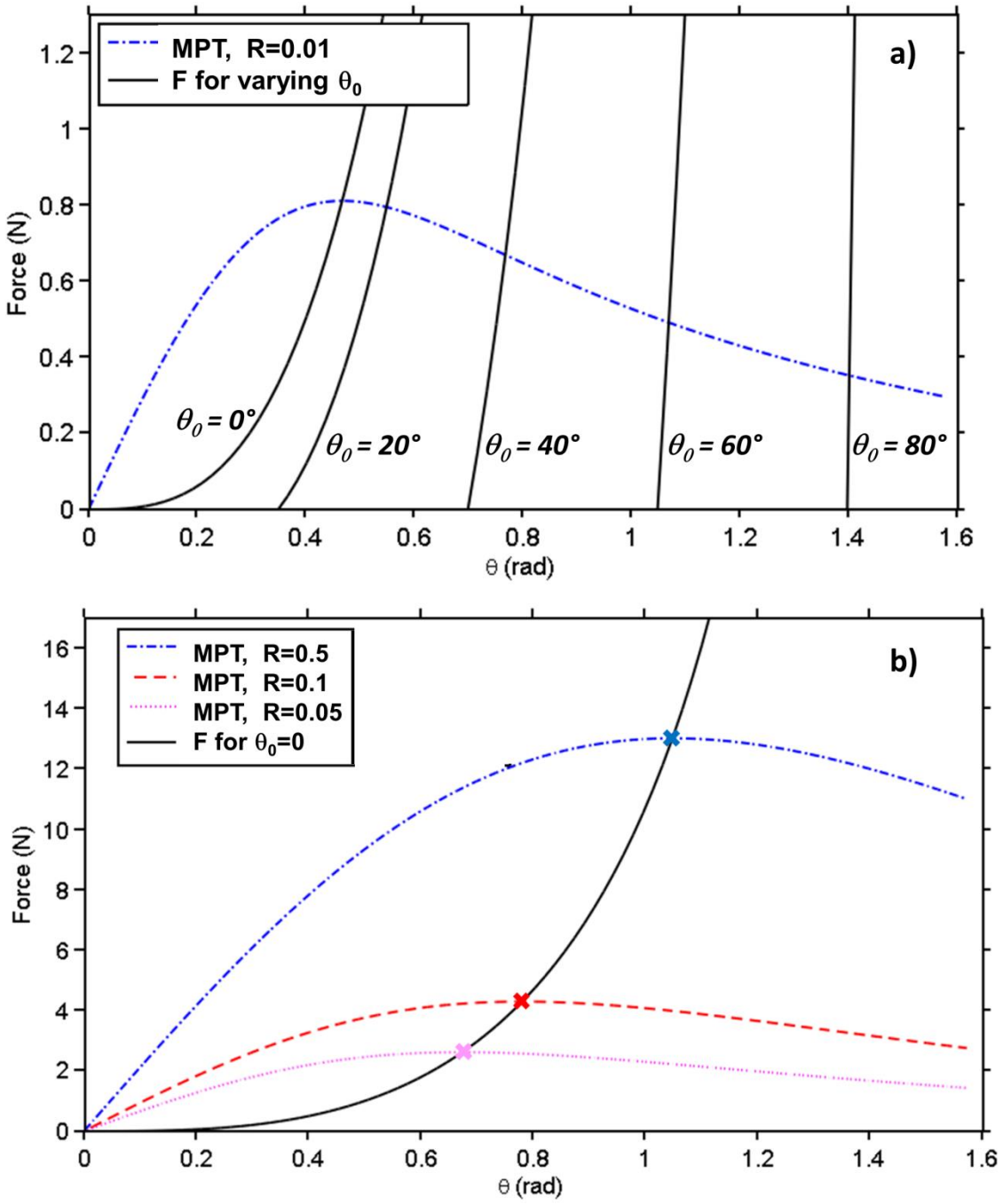

Fig. 3: External applied force F and tape peeling forces vs. peeling angle θ in symmetrical loading of a double-peeling symmetric configuration: a) R=0.01, varying θ_0;b) θ_0=0, varying R. The intersection between curves occurs for θ_0=0 at the maxima of the peeling force curves (indicated with crosses) i.e. for optimal peeling angle values.

The optimal peeling angle is a function of the global deformability of the system, i.e. the deformation that the system can sustain before delamination occurs. This property can be quantified by the non-dimensional parameter $\lambda = 2R/(tY)$, representing the ratio between adhesion energy and elasticity [14]. We thus wish to derive the optimal peeling angle as a function of λ. To analytically obtain the value of the optimal peeling angle and force for a given λ value, given by the intersection of the curves in Fig. 3, we must equate eqs. (4) and (6). With simple algebraic manipulation, we obtain

$$2\cos(\theta_{opt})^3 - (3+\lambda)\cos(\theta_{opt})^2 + 1 = 0 \qquad (7)$$

This equation can be solved for the non-dimensional parameter λ as a function of the optimal peeling angle θ_{opt}. Inverting the relation, we obtain the curve shown in Figure 4 for θ_{opt} vs. λ, showing a monotonically increasing nonlinear behaviour.

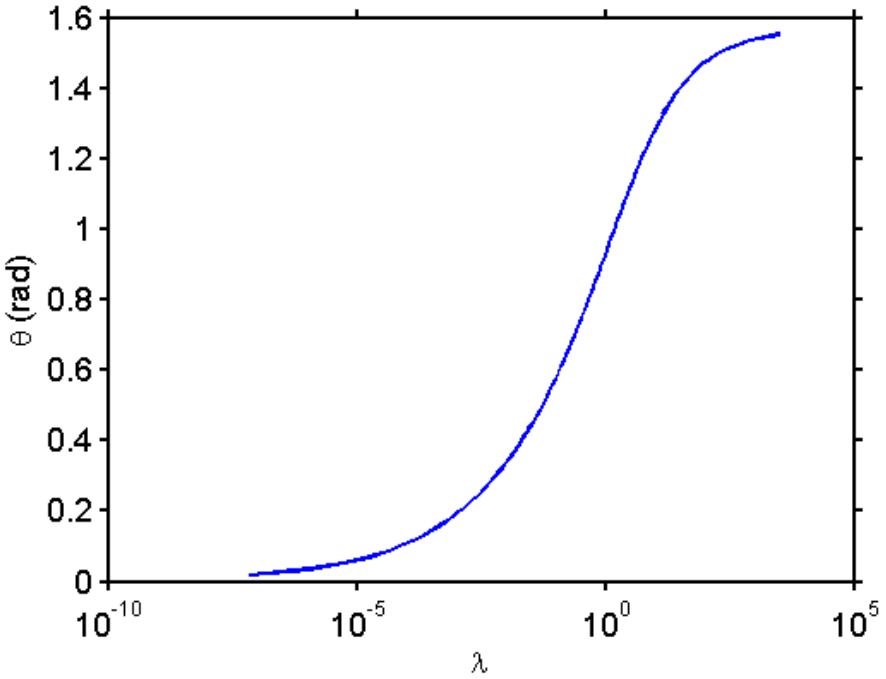

Fig. 4: Optimal peeling angle as a function of the non-dimensional parameter λ

3.2 Asymmetrical loading of a double peeling asymmetric configuration

Next, we consider an asymmetric structure loaded asymmetrically, i.e. with a non-vertical load. As an example, the following parameters are chosen for the structure: $l_1 + l_2 = l =$ 100mm, $\theta_1 = 40°$ $\theta_2 = 60°$ (initial angles) and $R = 0.001$ J/mm², while the tape's mechanical properties are the same as in the previous section. The parameter λ is of the order of 10^{-3}, so deformations at delamination are in this case very small. The delamination force calculated numerically as a function of the force application angle α is shown in Figure 5 (only the first delamination is considered). Here, the range considered for α corresponds to the cases where both tapes are in tension. The observed behaviour can be explained by the fact that the two tapes no longer delaminate simultaneously: starting from small angles, tape 1 delaminates while tape 2 does not, and for large angles the opposite happens. In correspondence with the

maximum of the curve, the symmetrical structure considered in the previous Section is obtained.

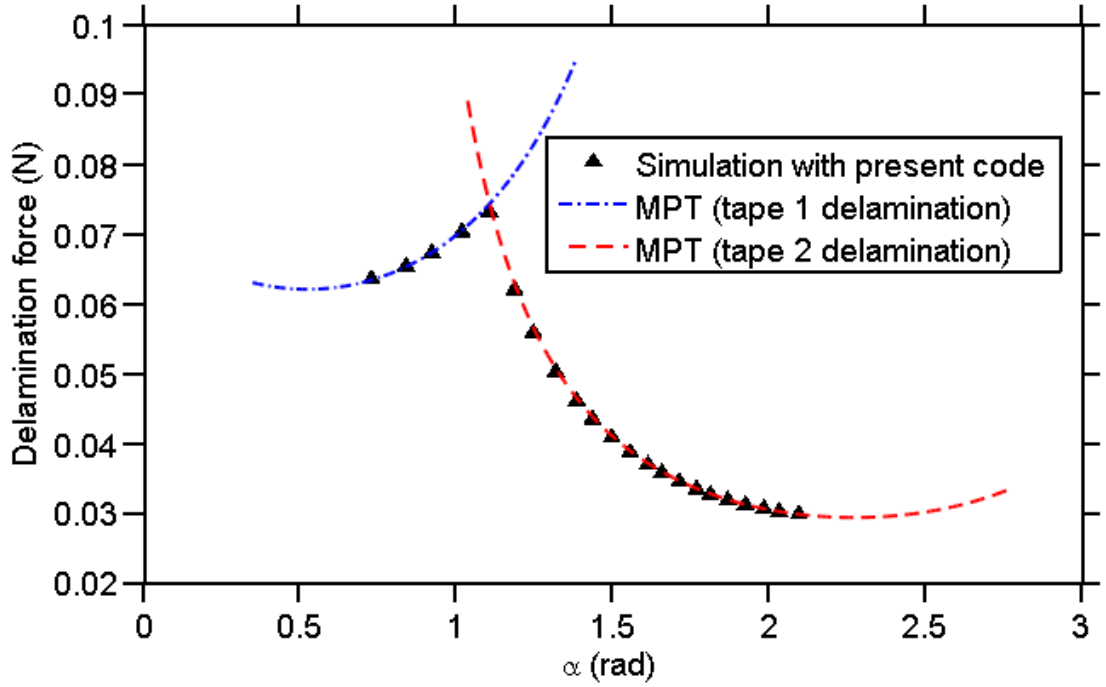

Fig. 5: Delamination force vs. applied force for a double peeling case for a quasi-rigid tape (small λ), calculated numerically (triangles) and by MPT (lines).

To better understand these results, we can consider the case when tape deformations are negligible (i.e. the limit case of tapes with small λ). Considering the force equilibrium on the tips of the tapes with this hypothesis, from Fig. 1 we have:

$$\begin{cases} F\cos(\alpha) - f_1\cos(\theta 1) + f_2\cos(\theta 2) = 0 \\ F\sin(\alpha) - f_1\sin(\theta 1) - f_2\sin(\theta 2) = 0 \end{cases} \tag{8}$$

where f_1 and f_2 are the reaction forces from tapes 1 and 2, respectively. It is now possible to write the relation between the two tape tensions:

$$f_1 \sin(\alpha - \theta 1) = f_2 \sin(\alpha + \theta 2) \quad (9)$$

Considering that only one of the tapes is delaminating, the corresponding delamination force is calculated using Kendall's equation. Using Eq. (9), it is possible to calculate the tension in the other tape, and using Eq. (8), the force applied to the system. Figure 5 shows that the simulation results (triangles) and the MPT solution (lines) coincide when the deformations are negligible.

The issue that remains to be clarified is now if the calculation of multiple peeling forces from a superposition of Kendall single peeling forces remains valid in the case of large deformations of the system. To verify this, simulations are performed with R=0.1 J/mm², so that λ is of the order of magnitude of 10^{-1}. Mechanical properties, total tape length and tape sections are the same as reported in the previous section. For various randomly chosen configurations, deformed angles and tensions in both tapes are numerically determined and compared to analytically calculated (using MPT) peeling forces. Table 1 shows typical results. The simulated peeling force of the delaminated tape can be obtained analytically if the deformed state (with corresponding angle modifications) is considered. For each considered configuration, and at each iterative simulation step, we find that the tension in the tape that delaminates is always equivalent to the peeling force obtained by analytical single peeling theory considering the deformed system, thus confirming the hypothesis of MPT.

	system 1	system 2	System 3
α (°)	75	100	60

θ1 initial (°)	40	40	45
θ2 initial (°)	60	60	45
θ1 deformed (°)	43.80	50.20	46.42
θ2 deformed (°)	76.44	63.60	65.84
Tape 1 tension (N)	2.10	0.85	**2.96**
Tape 2 tension (N)	**1.71**	**2.15**	0.80
External load (N)	3.21	2.62	3.33
MPT Peeling force tape 1 (N)	3.10	2.76	**2.96**
MPT Peeling force tape 2 (N)	**1.71**	**2.15**	2.06

Table 1: Tape tensions and corresponding angles compared to peeling forces calculated using MPT.

To better illustrate this, forces and deformations relative to system 1 in Table 1 are illustrated schematically in Fig. 6. Here, delamination occurs for one of the tapes (on the right), and the tape tension is therefore equal to the peeling force calculated using the single peeling theory as demonstrated by Multiple Peeling Theory. In this state, the tension in the other tape is smaller than the peeling force, and delamination does not take place.

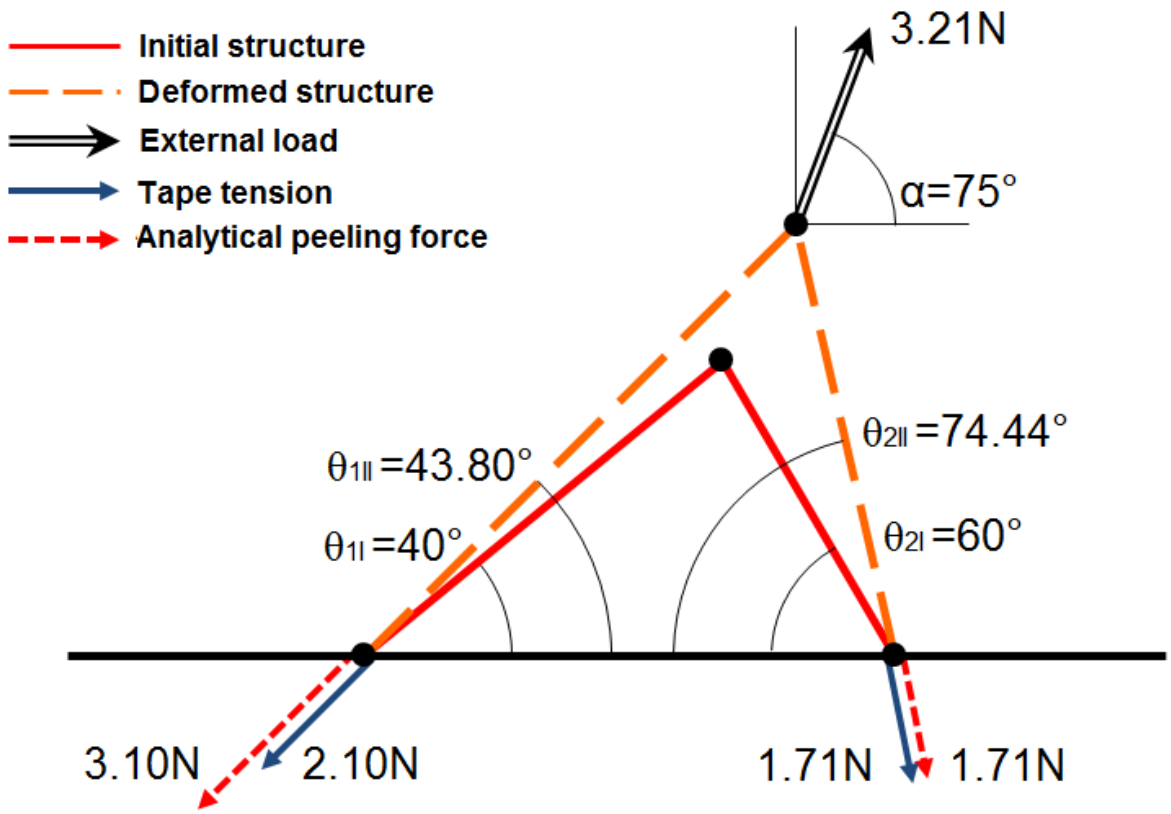

Fig. 6: Graphical representation of system 1 in Table 1, showing that numerically calculated peeling forces coincide with MPT-calculated ones where delamination occurs, if the deformed configuration is considered.

3.3 Simulations of delamination evolution

We now consider the same structures considered previously, simulating the peeling phase beyond the first delamination, i.e. the entire detachment process. The same mechanical properties as in the previous sections are used, with R=0.01 J/mm². The structure is symmetric and the total tape length is l=20 mm at the onset of the simulation. Figure 7a shows the force and the peeling angle as a function of the vertical tip displacement. Starting from θ=90°, simulations show that the peeling force grows and tends to a limit value, and simultaneously the peeling angle decreases and also tends to a limit value. The structure becomes optimal for this peeling angle value, since the delamination force is maximal. The behaviour obtained simulating the entire process is equivalent to that obtained calculating single delaminations at various peeling angles. On the other hand, if we start from θ = 0 (Fig. 7b), it can be seen that an abrupt slope change occurs for both force and peeling angle after the first delamination, after which both remain constant in the subsequent delamination phase, since the optimal force and angle have already been reached.

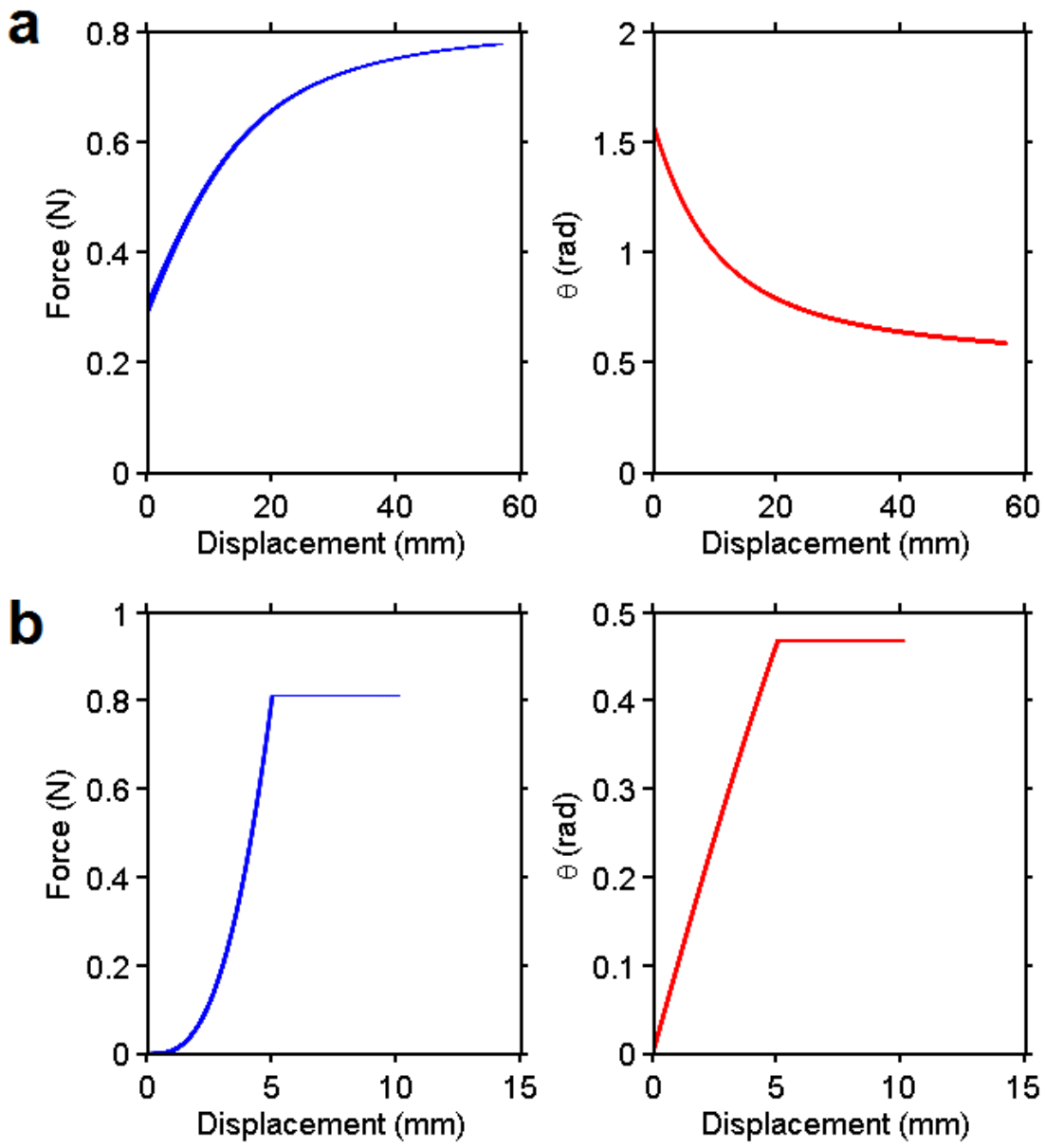

Fig. 7: Delamination force and peeling angle as a function of the vertical tip displacement in a symmetrical double peeling simulation, a) starting from θ = 90° *(1.57 rad). b) starting from* θ = 0.

In the asymmetric case, we have verified that there is an optimal force direction at the tip of the tapes, depending on the geometry of the structure. If we now simulate the entire detachment process starting from the previous geometry, adopting a non-optimal force direction, the progressive delamination leads to a modification of the geometry in order to reach the equilibrium with both tapes under critical tension. Figure 8 shows the force as a function of the peeling angle for the two tapes. These curves are divided in two parts: the first (A-B) corresponds to a single-tape delamination phase necessary for the system to reach equilibrium, at which both tapes start delaminating together, and the second (B-C) to a phase in which the system reaches optimal angles.

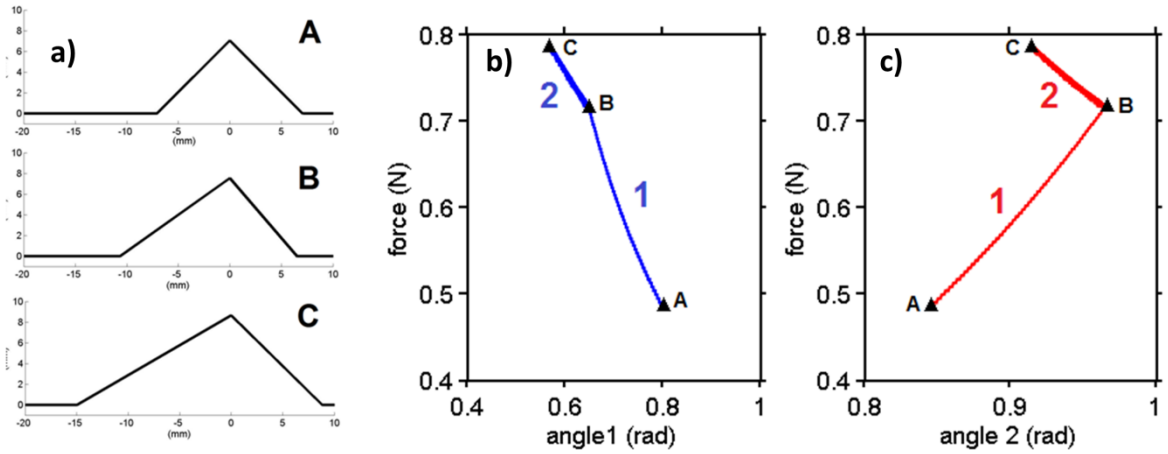

Fig. 8: Delamination phases in a symmetrical double peeling simulation with a non-vertical force: a) configuration at three successive time steps: A, B, and C; b) corresponding force vs. peeling angle on the left tape; c) corresponding force vs. peeling angle on the right tape.

All results in the previous sections are relative 2D geometries. However, this 2D model is applicable to 3D geometries in which the delamination force lies in a plane perpendicular to the surface. To extend the approach to more general 3D cases, an additional angle would be

necessary to describe the direction in space of the applied load, and in some cases a further angle describing the direction of the non-delaminated tapes with respect to delaminated ones (the two directions do not necessarily coincide). The problem can be treated, analytically and numerically, in a similar way to that illustrated above, and peeling force surfaces (instead of curves) can be obtained e.g. as a function of the multiple angles mentioned above. Work is under way to study this problem, but the topic is beyond the scope of this paper.

4. Spider web anchorages

Spiders attach their silk draglines to substrates using so called attachment discs [20]. These structures involve pyriform silk coated with a fluid that favours adhesion [21]. Recent studies have discussed the mechanics of different spider anchorages [18, 19]: two main structures can be observed, with different functions. The first is a so-called "staple-pin" structure ("scaffolding" silk, Fig.9a), where branches are aligned and initially fully attached to the substrate, resulting in a plane morphology, which is used as a structural anchorage. Figure 9b shows a detail of a fluid-coated silk fibre: notice the similarity with the adhesive tape considered in the previous section. The other possible architecture is a so-called "dendritic" structure ("gumfoot" silk), which can be described as a radial branching structure where the pyriform silk fibres converge to a single point at a distance from the substrate, resulting in a cone-like morphology (Fig. 9c) which is involved in spider prey capture. It has been shown [18, 19] that although they are based on the same pyriform silk, the two structures exhibit very different mechanical behaviour, which is functional to their role. To perform its function, the staple-pin anchorage must display high detachment strength, whilst the dendritic anchorage must exhibit a reduced pull off force.

The first element that can explain the different pull off forces observed for the two structures is the different extent of contact splitting occurring in the two morphologies. It is well known [7, 8] that a larger number of contacts occurring in the pyriform silk implies a greater peeling line, and therefore a higher delamination strength. However, we will show in this section that other mechanisms related to the architecture of the anchorages can explain the differences between their different behaviour and maximal pull off force.

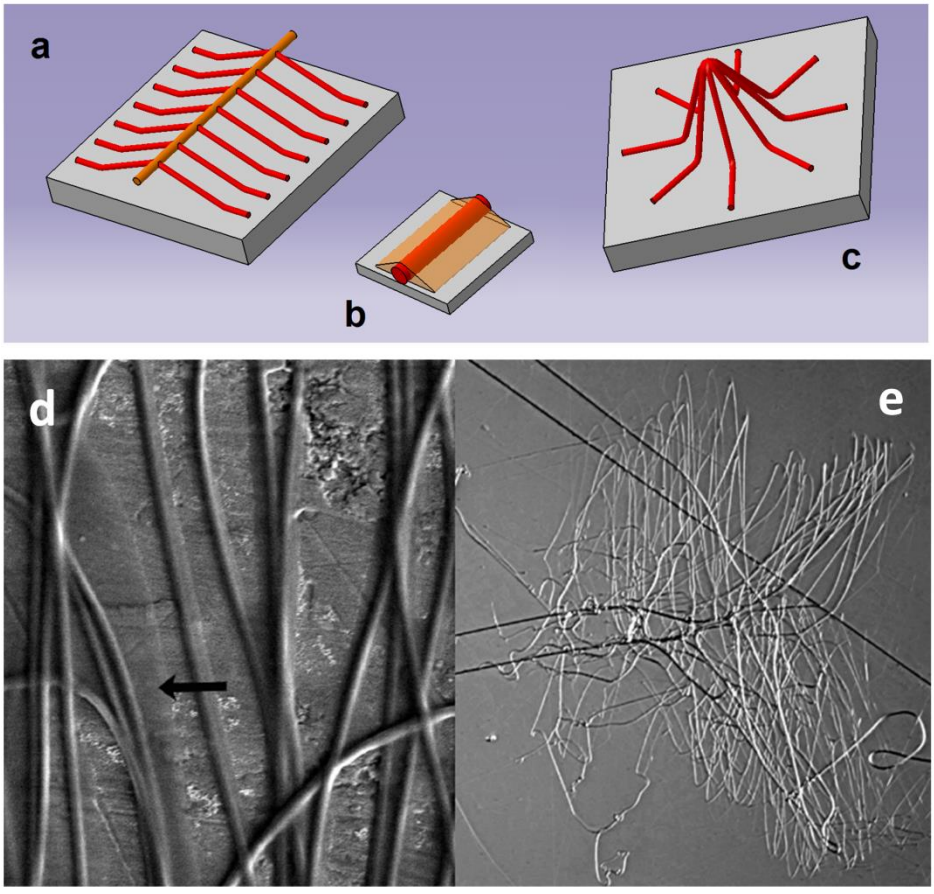

Fig. 9: Spider silk attachment structures: a) schematic of a "staple-pin" architecture; b) detail of a fluid-coated silk fibre; c) schematic of a "dendritic" architecture; d) optical micrograph of spider web generic anchorage (from [22]) also showing details of the fluid-coated silk fibre (indicated by an arrow); e) optical micrograph of a staple pin anchorage.

The simulations reported here use the same mechanical properties as in the previous Section, with an adhesive energy of R=0.01 J/mm^2. Since the approach is qualitative and only means to evaluate the role of geometry, results can be extended to any system with equivalent morphology and rigidity.

Firstly, we will consider the dendritic anchorage. Due to its conical symmetry, the relationship between force and extension can be directly obtained from the symmetric double peeling configuration described in Section 3.1, modified by multiplying results by the appropriate number of tapes. As observed previously, in order to obtain a smaller delamination force, the initial tape angle must be close to θ = 90°. Figure 10a shows simulations results for various dendritic attachments with a varying number of tapes N, for the same initial tape angles (θ = 90°) and for a distance between substrate and the anchorage tip (i.e. detached tape length) of l_i=10 mm. Clearly, the pull-off force is proportional to the number of contacts. The system is firstly deformed without delamination, with a linear force-displacement relationship (Hooke's law). Then, the tapes begin to delaminate and the peeling angle starts to vary, which results in an increase of the peeling force. This explains the elasto-plastic-like behaviour obtained in experimental [18] and numerical (Fig 10) results. The peeling force saturates when the peeling angle is optimal. Exploiting this fact, it is clear that it is possible to maintain a small peeling force by increasing the initially detached tape lengths, since the displacement (and delamination length) necessary to reach the optimal configuration is greater. This is shown in Fig. 10b, where force-displacement curves are compare for the same number of tapes but varying detached length. Thus, for a given delamination length, increasing the anchorage length (i.e. detached tape length) and using small initial angles are structural strategies that allow to limit the pull-off force and obtain "weak" anchorages.

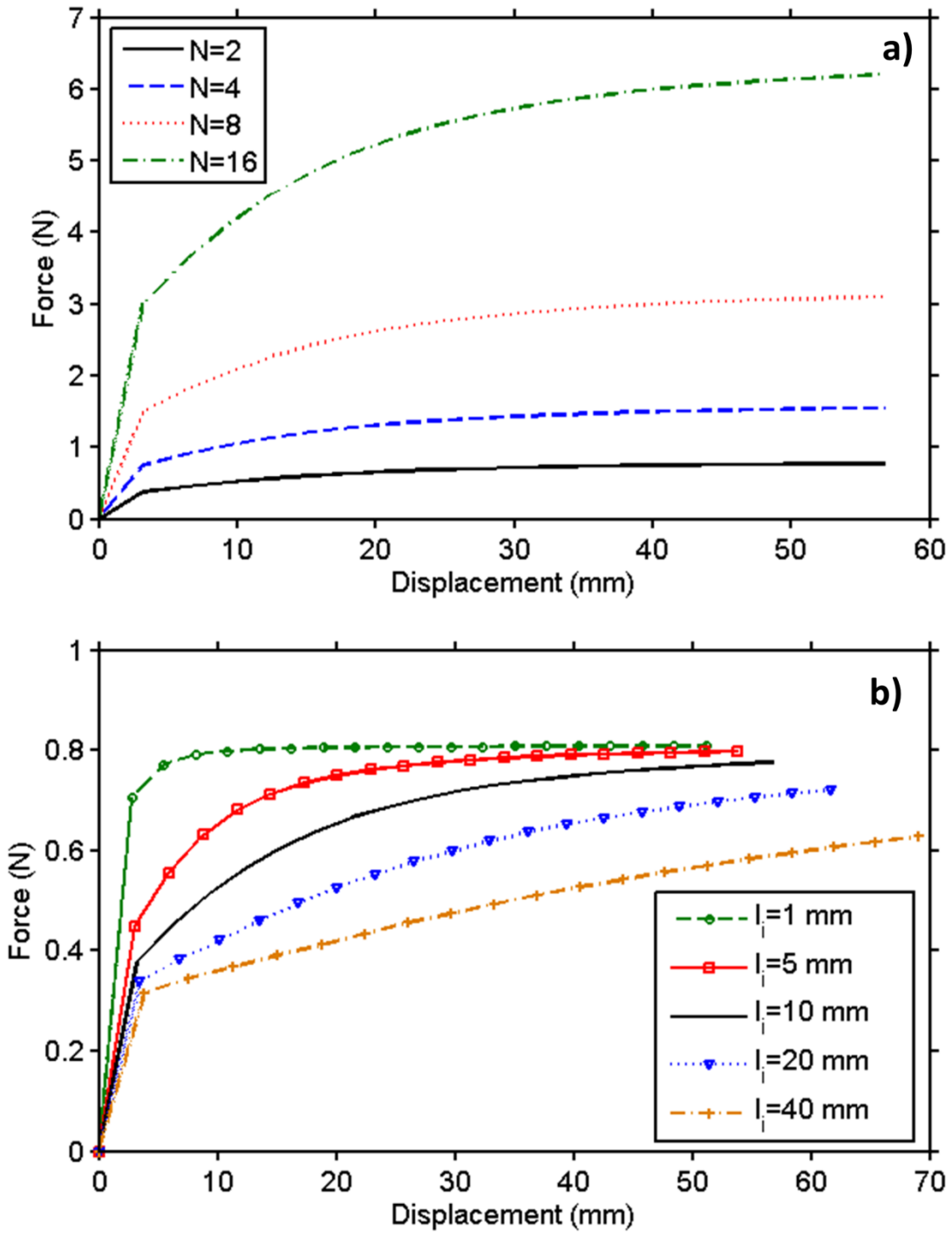

Fig. 10: Force-extension curves for a dendritic anchorage, for a) varying number N of fibres in the anchorage (l_i=10 mm), and b) varying detached length l_i of the anchorage (N=2).

The staple-pin anchorage, on the other hand, can be approximated by a succession of parallel symmetric double tapes (Fig. 11). The first observation regarding this system is that the displacement or force application point is adjacent to the substrate. Therefore, the initial angle of all double-tapes is close to zero. This provides a configuration which requires a greater pull-off force than the dendritic system, since it is close to the optimal configuration, as explained in Section 3 (optimal deformed peeling angles correspond to zero initial angles). To simulate the anchorage during the delamination process, we assume that a displacement is imposed on the first double-tape, and that the following double-tape displacement depends on the first one. Considering a quasi-rigid dragline, successive displacements linearly decrease with respect to the first one, as shown in Fig. 11 (side views).

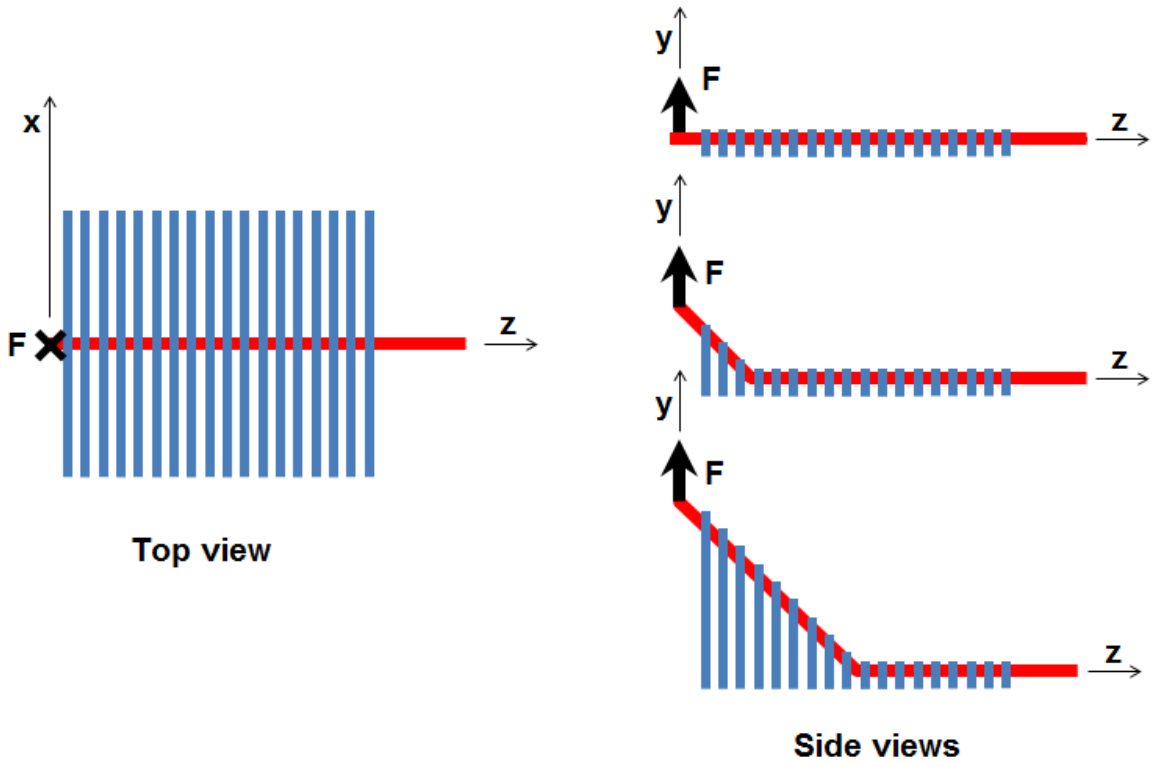

Fig. 11: Schematic of the delamination mechanism in a staple-pin anchorage.

If we indicate with dy_1 the displacement of the first double-tape tip, the successive displacements are given by:

$$dy_j = dy_1 - Cz_j \tag{10}$$

where dy_j are the imposed displacements of the j-th double tapes, z_j the positions of the j-th double tapes along the z axis in Fig. 11 and C is a constant that can be derived from Eq. (10) from the imposed displacements. In the simulation, each tape edge is coincident with the previous and the succeeding one, and tape centers are separated by b=15 mm. The total number of double tapes in the system is N = 6, the initial tape length is 1 mm and initial tape angle is 0. Figure 12 shows the delamination force as a function of the imposed displacement, with C=1/15. It is apparent that the curve is the superposition of the delamination forces of the double tapes involved in the deformation of the system. Since C is relatively small, the first tape deforms and begins to delaminate; when it reaches a certain displacement value, the successive double tape begins to deform and delaminate, and so on. The reaction force is thus the sum of optimal peeling forces of the single delaminating tapes, which explains the step-like behaviour. The number of plateaus in the curve is equal to the number of double tapes in the structure. When all 6 double tapes are delaminating, the force is maximal and remains constant.

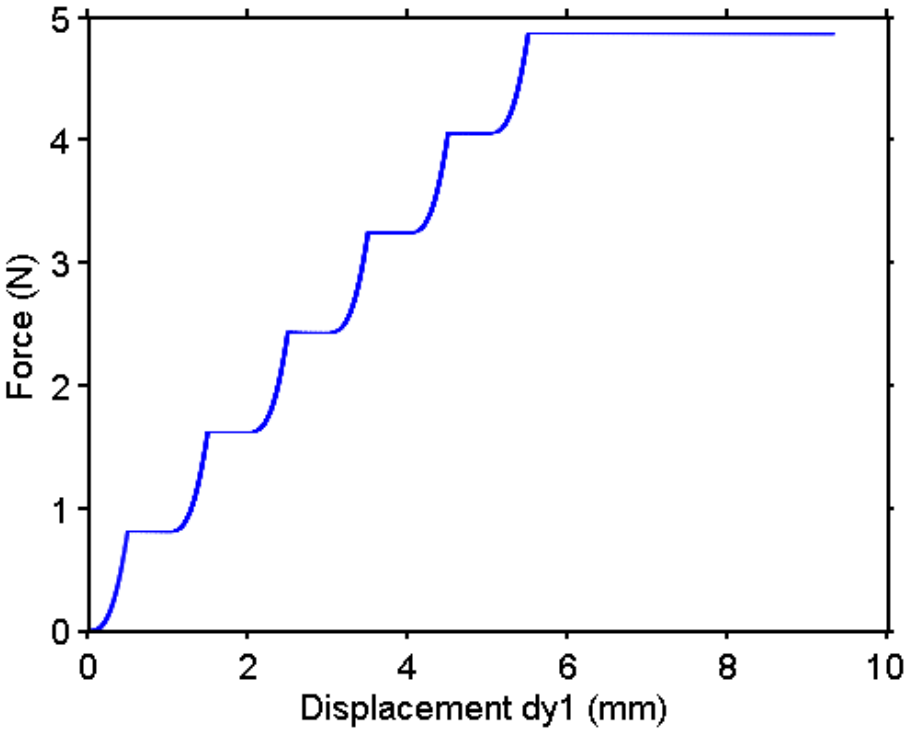

Fig. 12: Force-extension curves for a staple-pin anchorage

A further example of geometrical feature which contributes to the optimization of the adhesive strength of this type of anchorage can be observed by considering the high density of pyriform silk fibers in the staple–pin morphology (Fig. 9e), and the fact that the coating fluid contact area with the substrate is considerably larger than the dimension of the fiber (Fig. 9d). Thus, we can assume that the contact between the structure and the substrate is continuous in the *z* direction, i.e. there are no gaps between the contact areas of the different double tapes. The structure with gaps (above) and without (below) is shown schematically in Fig. 12. In the latter case, the peeling line is not parallel to the z direction, and is thus not equal for all detached tapes at a given delamination length of the dragline silk. The peeling length increases with the angle between the two peeling lines and the *z* axis, which in turn increases

with the delaminated length of the dragline silk. Hence, the total peeling length and peeling force increase with the delamination length.

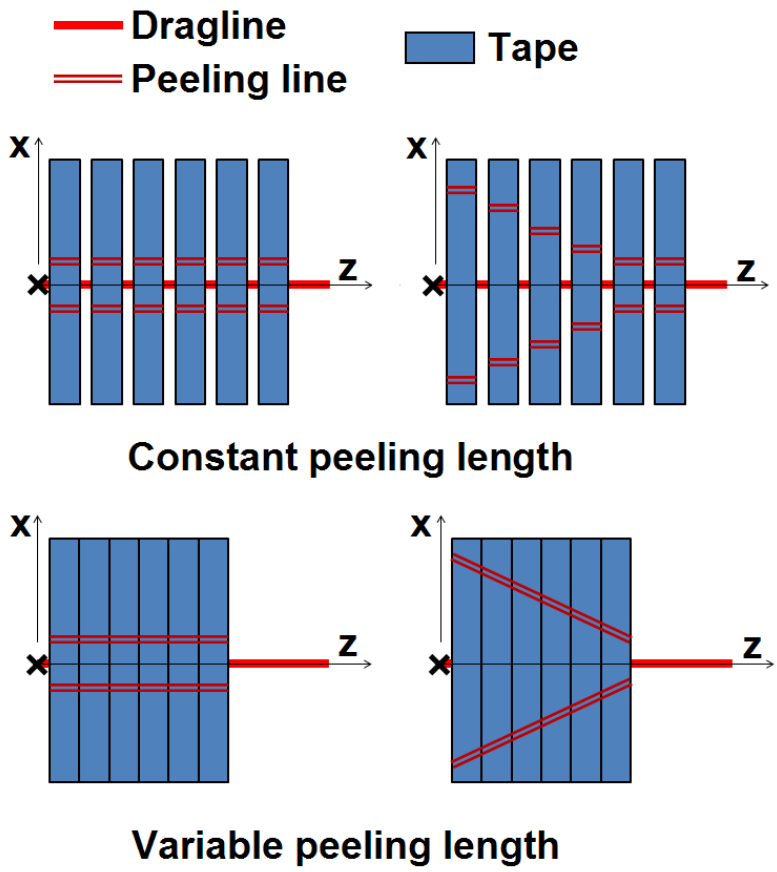

Fig. 13: Mechanism for increasing the peeling length (and force) in a staple-pin anchorage: the peeling line increases its angle with respect to z as the delamination proceeds along z

Thus, we have shown that using geometry only, the spider can tune and optimize the shape of the force-displacement curves of web anchorages, and thus generate different optimized constitutive laws for achieving specific functionalities (e.g. from stable/strong anchorages for attachment to instable/weak anchorages for capturing).

5. Conclusions

We have developed a new numerical approach to simulate the peeling behaviour of multiple fibrillar adhesives. We have validated the model using known results from MPT [14], and shown that it can provide further predictions for asymmetrical or arbitrarily complex configurations. In particular, the model has been used to prove a previously postulated "ansatz", namely that all multiple peeling problems can be solved as a superposition of Kendall single peeling configurations, provided they are applied to the appropriate deformed state of the system, as stated by MPT and already demonstrated for symmetric double peeling [14]. Finally, we have applied the new numerical model to study the specific adhesive properties of two distinct spider web anchorage types, showing how their structural features are instrumental in defining their constitutive law and overall adhesive strength, and therefore their effectiveness in accomplishing their function.

Acknowledgements:

This work was carried out within the COST Action TD0906 on Biological Adhesives. NMP is supported by the European Research Council (ERC StG Ideas 2011 BIHSNAM n. 279985 on "Bio-Inspired hierarchical super-nanomaterials", ERC PoC 2013-1 REPLICA2 n. 619448 on "Large-area replication of biological anti-adhesive nanosurfaces", ERC PoC 2013-2 KNOTOUGH n. 632277 on "Super-tough knotted fibres"), by the European Commission under the Graphene Flagship (WP10 "Nanocomposites", n. 604391) and by the Provincia Autonoma di Trento ("Graphene Nanocomposites", n. S116/2012-242637 and reg.delib. n. 2266). LB and FB acknowledge support from BIHSNAM.

References

[1] Smith, A.M. & Callow, J.A. 2006 *Biological adhesives*. Berlin ; New York, Springer.

[2] Autumn, K. & Peattie, A.M. 2002 Mechanisms of adhesion in geckos. *Integrative and Comparative Biology* **42**, 1081-1090 (doi: 10.1093/icb/42.6.1081).

[3] Yao, H. & Gao, H. 2006 Mechanics of robust and releasable adhesion in biology: Bottom–up designed hierarchical structures of gecko. *Journal of the Mechanics and Physics of Solids* **54**, 1120-1146. (doi:10.1016/j.jmps.2006.01.002).

[4] Sahni, V., Blackledge, T.A. & Dhinojwala, A. 2011 A Review on Spider Silk Adhesion. *The Journal of Adhesion* **87**, 595-614. (doi:10.1080/00218464.2011.583588).

[5] Arzt, E., Gorb, S. & Spolenak, R. 2003 From micro to nano contacts in biological attachment devices. *Proceedings of the National Academy of Sciences* **100**, 10603-10606. (doi:10.1073/pnas.1534701100).

[6] Pugno, N.M. & Lepore, E. 2008 Living Tokay Geckos Display Adhesion Times Following Weibull Statistics. *Journal of Adhesion* **84**, 949-962. (doi:10.1080/00218460802505374).

[7] Varenberg, M., Pugno, N.M. & Gorb, S.N. 2010 Spatulate structures in biological fibrillar adhesion. *Soft Matter* **6**, 3269-3272. (doi: 10.1039/C003207g).

[8] Kamperman, M., Kroner, E., del Campo, A., McMeeking, R.M. & Arzt, E. Functional Adhesive Surfaces with “Gecko” Effect: The Concept of Contact Splitting. *Advanced Engineering Materials* **12**, 335-348. (doi:10.1002/adem.201000104).

[9] Geim, A.K., Dubonos, S.V., Grigorieva, I.V., Novoselov, K.S., Zhukov, A.A. & Shapoval, S.Y. 2003 Microfabricated adhesive mimicking gecko foot-hair. *Nature Materials* **2**, 461-463 (doi:10.1038/nmat917).

[10] Carbone, G., Pierro, E. & Gorb, S.N. 2011 Origin of the superior adhesive performance

of mushroom-shaped microstructured surfaces. *Soft Matter* **7**, 5545-5552. (doi:10.1039/C0SM01482F).

[11] Piccardo, M., Chateauminois, A., Fretigny, C., Pugno, N.M. & Sitti, M. 2013 Contact compliance effects in the frictional response of bioinspired fibrillar adhesives. *Journal of The Royal Society Interface* **10**. (doi:10.1098/rsif.2013.0182).

[12] Kovalev, A.E., Varenberg, M. & Gorb, S.N. 2012 Wet versus dry adhesion of biomimetic mushroom-shaped microstructures. *Soft Matter* **8**, 7560-7566. (doi:10.1039/C2SM25431J).

[13] Pugno, N.M. 2008 Spiderman gloves. Nano Today 3, 35-41. (doi: 10.1016/S1748-0132(08)70063-X).

[14] Pugno, N.M. 2011 The theory of multiple peeling. *International Journal of Fracture* **171**, 185-193. (doi:10.1007/s10704-011-9638-2).

[15] Afferrante, L., Carbone, G., Demelio, G. & Pugno, N. 2013 Adhesion of Elastic Thin Films: Double Peeling of Tapes Versus Axisymmetric Peeling of Membranes. *Tribol Lett* **52**, 439-447. (doi:10.1007/s11249-013-0227-6).

[16] Kendall, K. 1975 Thin-film peeling-the elastic term. *Journal of Physics D: Applied Physics* **8**, 1449 (doi:10.1088/0022-3727/8/13/005).

[17] Gorb, S.N. 2008 Biological attachment devices: exploring nature's diversity for biomimetics. *Philosophical Transactions of the Royal Society A: Mathematical, Physical and Engineering Sciences* **366**, 1557-1574. (doi:10.1098/rsta.2007.2172).

[18] Sahni, V., Harris, J., Blackledge, T.A. & Dhinojwala, A. 2012 Cobweb-weaving spiders produce different attachment discs for locomotion and prey capture. *Nat Commun* **3**, 1106. (doi: 10.1038/ncomms2099).

[19] Cranford, S.W., Tarakanova, A., Pugno, N.M. & Buehler, M.J. 2012 Nonlinear material

behaviour of spider silk yields robust webs. *Nature* **482**, 72-76. (doi: 10.1038/nature10739).

[20] Sahni, V., Blackledge, T.A. & Dhinojwala, A. A Review on Spider Silk Adhesion. *The Journal of Adhesion* **87**, 595-614. (doi:10.1080/00218464.2011.583588).

[21] Sahni, V., Blackledge, T.A. & Dhinojwala, A. Viscoelastic solids explain spider web stickiness. *Nat Commun* **1**, 19 (doi:10.1038/ncomms1019).

[22] Pugno, N.M., Cranford, S.W. & Buehler, M.J. 2013 Synergetic Material and Structure Optimization Yields Robust Spider Web Anchorages. *Small* **9**, 2747-2756. (doi:10.1002/smll.201201343).